Biomedical Optics EXPRESS

In vitro hematocrit measurement using spectrally encoded flow cytometry

ADEL ZEIDAN, LIOR GOLAN, AND DVIR YELIN*

Faculty of Biomedical Engineering, Technion—Israel Institute of Technology, Haifa 3200003, Israel
*yelin@bm.technion.ac.il

Abstract: Measuring key physiological parameters of small blood samples extracted from patients could be useful for real-time clinical diagnosis at the point of care. An important parameter required from all blood tests is the blood hematocrit, a measure of the fractional volume occupied by the red cells within the blood. In this work, we present a method for *in vitro* evaluation of hematocrit based on the data acquired using spectrally encoded flow cytometry. Analysis of the reflectance confocal images of blood within a flow chamber resulted in an error as low as 1.7% in the measured hematocrit. The technique could be used as part of an *in vitro* diagnostic system that measures important blood parameters at the point of care.

©2016 Optical Society of America

OCIS codes: (170.1790) Confocal microscopy; (170.1470) Blood or tissue constituent monitoring; (170.1530) Cell analysis.

References and links

1. H. Billett, "Hemoglobin and Hematocrit," in *Clinical Methods: The History, Physical, and Laboratory Examinations.*, H. W. Walker, H. K. Hurst, ed. (Butterworths, Boston, 1990).
2. J. G. Quinn, E. A. Tansey, C. D. Johnson, S. M. Roe, and L. E. A. Montgomery, "Blood: tests used to assess the physiological and immunological properties of blood," Adv. Physiol. Educ. **40**(2), 165–175 (2016).
3. W. S. Chen, H. H. Zhu, and G.-S. Feng, "Treating leukemia at the risk of inducing severe anemia," Exp. Hematol. **44**(5), 329–331 (2016).
4. B. J. Stuart and A. J. Viera, "Polycythemia vera," Am. Fam. Physician **69**(9), 2139–2144 (2004).
5. C. R. Kjeldsberg, *Practical Diagnosis of Hematologic Disorders* (ASCP Press, 2000).
6. J. Y. Vis and A. Huisman, "Verification and quality control of routine hematology analyzers," Int. J. Lab. Hematol. **38**(Suppl 1), 100–109 (2016).
7. D. Heikali and D. Di Carlo, "A Niche for Microfluidics in Portable Hematology Analyzers," J. Assoc. Lab. Autom. **15**(4), 319–328 (2010).
8. Y. Ben-Yosef, B. Marom, G. Hirshberg, C. D'Souza, A. Larsson, and A. Bransky, "The HemoScreen, a novel haematology analyser for the point of care," J. Clin. Pathol. **69**(8), 720–725 (2016).
9. S. Capiau, L. S. Wilk, M. C. G. Aalders, and C. P. Stove, "A Novel, Nondestructive, Dried Blood Spot-Based Hematocrit Prediction Method Using Noncontact Diffuse Reflectance Spectroscopy," Anal. Chem. **88**(12), 6538–6546 (2016).
10. S. Oshima and Y. Sankai, "Optical measurement of blood hematocrit on medical tubing with dual wavelength and detector model," in *2009 Annual International Conference of the IEEE Engineering in Medicine and Biology Society*, (2009), 5891–5896.
11. M. Jędrzejewska-Szczerska, M. Gnyba, and M. Kruczkowski, "Low-coherence method of hematocrit measurement," in *2011 Federated Conference on Computer Science and Information Systems (FedCSIS)*, (2011), 387–391.
12. E. F. Treo, D. O. Cervantes, C. J. Felice, M. Tirado, and M. E. Valentinuzzi, "Hematocrit measurement by dielectric spectroscopy," in *Engineering in Medicine and Biology, 2002. 24th Annual Conference and the Annual Fall Meeting of the Biomedical Engineering Society EMBS/BMES Conference, 2002. Proceedings of the Second Joint*, (2002), 1750–1751 **vol.1752**.
13. D. Trebbels, R. Zengerle, and D. Hradetzky, "Hematocrit Measurement - A high precision on-line measurement system based on impedance spectroscopy for use in hemodialysis machines," in *World Congress on Medical Physics and Biomedical Engineering, September 7 - 12, 2009, Munich, Germany: **Vol. 25**/7 Diagnostic and Therapeutic Instrumentation, Clinical Engineering*, O. Dössel and W. C. Schlegel, eds. (Springer Berlin Heidelberg, Berlin, Heidelberg, 2009), pp. 247–250.
14. J. Steinfelder-Visscher, P. W. Weerwind, S. Teerenstra, G. A. M. Pop, and R. M. H. J. Brouwer, "Conductivity-Based Hematocrit Measurement During Cardiopulmonary Bypass," J. Clin. Monit. Comput. **21**(1), 7–12 (2007).
15. W. Secomski, A. Nowicki, and P. Tortoli, "Estimation of hematocrit by means of attenuation measurement of ultrasonic wave in human blood," in *Ultrasonics Symposium, 2001 IEEE*, (2001), 1277–1280 **1272**.

#272036 http://dx.doi.org/10.1364/BOE.7.004327
Journal © 2016 Received 20 Jul 2016; revised 11 Sep 2016; accepted 14 Sep 2016; published 27 Sep 2016

Biomedical Optics EXPRESS

16. L. Golan and D. Yelin, "Flow cytometry using spectrally encoded confocal microscopy," Opt. Lett. **35**(13), 2218–2220 (2010).
17. L. Golan, D. Yeheskely-Hayon, L. Minai, E. J. Dann, and D. Yelin, "Noninvasive imaging of flowing blood cells using label-free spectrally encoded flow cytometry," Biomed. Opt. Express **3**(6), 1455–1464 (2012).
18. L. Golan, D. Yeheskely-Hayon, L. Minai, and D. Yelin, "High-speed interferometric spectrally encoded flow cytometry," Opt. Lett. **37**(24), 5154–5156 (2012).
19. A. Zeidan and D. Yelin, "Reflectance confocal microscopy of red blood cells: simulation and experiment," Biomed. Opt. Express **6**(11), 4335–4343 (2015).
20. A. Lovell, J. C. Hebden, J. C. Goldstone, and M. Cope, "Determination of the transport scattering coefficient of red blood cells," in *BiOS'99 International Biomedical Optics Symposium*, (International Society for Optics and Photonics, 1999), 175–182.
21. T. K. Gebretsadkan, G. Ambachew, and H. Birhaneselassie, "The Comparison between Microhematocrit and Automated Methods for Hematocrit Determination," Int. J. Blood Res. Disord. **2**, 012 (2015).
22. H. Chaplin, Jr. and P. L. Mollison, "Correction for plasma trapped in the red cell column of the hematocrit," Blood **7**(12), 1227–1238 (1952).

1. Introduction

The hematocrit (HCT), i.e. the volume percentage of red blood cells in the blood, is an important clinical index that provides invaluable information on the patient's health. Low HCT levels may indicate various types of anemia [1] that point to nutritional (iron, folate and vitamins) deficiencies, malnutrition, blood loss, increased erythrocytes destruction [2], or leukemia treatment [3]. Elevated HCT levels may point to conditions including polycythemia vera [4, 5], dehydration, erythrocytosis, or other disorders associated with plasma volume loss [2, 4]. The most common approach for determining HCT is multiplying the red blood cell (RBC) count by the mean cell volume (MCV), both parameters are directly measured by an automated hematology analyzer [6]. These analyzers employ optical flow cytometry that uses hydrodynamic [7] or viscoelastic [8] focusing of stream of blood cells to quantify numerous parameters of the cells through light scattering, absorption, and fluorescence. In low resource environments, where automated analyzers are not readily available, HCT is often measured directly using centrifugation that separates the plasma from the packed RBCs. *In vitro* measurement of HCT have also been demonstrated using various optical techniques, including measuring the reflectance from dried blood spots [9], analyzing light scattering from blood samples [10], and using low-coherence interferometry [11]. Non-optical techniques for measuring HCT *in vitro* include dielectric [12] and impedance [13] spectroscopy, conductivity-based measurements [14] and ultrasonic attenuation [15].

Recently, a method for imaging cells in flow, termed spectrally encoded flow cytometry (SEFC) [16], has been demonstrated promising for blood cytometry. Using a diffraction grating and a high numerical-aperture objective lens to image a single transverse line within a flow chamber, SEFC provided 2D reflectance confocal images of label-free cells without any mechanical scanning. SEFC has been demonstrated promising for counting blood cells *in vivo* [17, 18] and for measuring RBC corpuscular volume *in vitro* [19]. In this work, we demonstrate a method for *in vitro* HCT measurement using SEFC. Following system calibration with artificially made blood samples of various hematocrit levels, the method was tested by measuring the mean brightness and the coefficient of variation of the SEFC images of blood samples from eight patients. Depending on the exact analysis approach, the results show errors between 1.7% and 4.3% when compared to centrifugation-based measurement.

2. Experiment

A beam of broadband light from a fiber-coupled super-luminescent diode (SLD) array (Superlum S840-B-I-20, 840 nm center wavelength, 53 nm bandwidth) was collimated using an aspheric lens (11 mm focal length, L1), magnified by an achromatic lens pair (–20 mm and 75 mm focal lengths for lenses L3 and L4, respectively), diffracted by a transmission grating (1200 lines/mm, Wasatch photonics), and imaged using a 1x telescopic arrangement (L5 and L6, 75 mm focal length) onto the entrance pupil of a × 60 water-immersion NA = 1.2 objective lens (Olympus). Light reflected back from the sample was collected through the

Biomedical Optics EXPRESS

same optical path and deflected by a cubic beam-splitter into a single-mode fiber using an aspheric lens (11 mm focal length, L2). The spectrum of the reflected light was measured by a custom-built spectrometer using 75-mm-focal-length achromatic collimation lens, 1200 lines/mm transmission grating, 250-mm-focal-length lens and a 2048-pixel line camera (SPL2048-70km, Basler). Note that the spectral measurement described here is used for measuring the intensity of the reflections along a lateral axis within the flow chamber, and is not used for encoding depth or for evaluating the spectrum of the reflected light.

Blood samples from eight volunteers (Helsinki approval #0068-11) were drawn into a collection tube containing an anticoagulant (K2-EDTA). For system calibration, 15 ml of each blood sample was added to a test tube containing 15 ml of a density gradient medium (Lymphoprep, STEMCELL Technologies) and centrifuged for 20 minutes at 1200g in room temperature. The plasma layer and the RBC pellet were collected separately and mixed together into ten different concentrations to obtain the calibration set comprising of HCT levels between 15% and 60% with 5% intervals (Fig. 1). The remaining portion of the whole blood was used for control HCT measurements using centrifugation, and for imaging by our SEFC system, where the blood sample was pushed at a velocity of 4 mm/s by a syringe pump (Syringe pump 11 Elite, Harvard Apparatus) through a rectangular 5 mm x 0.2 mm cross section flow channel (μ-Slide $I^{0.2}$ Luer, Ibidi). The flow channel was mounted onto a computer-controlled linear translation stage (M-683.2U4, Physik Instrumente) and was step-scanned in the axial dimension for imaging at different depths within the flow chamber.

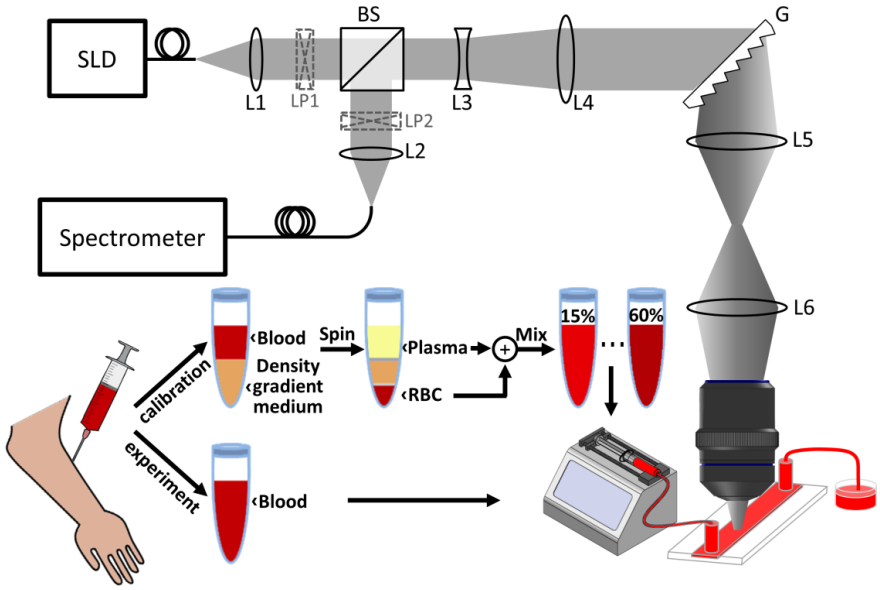

Fig. 1. Schematic illustration of the *in vitro* SEFC system. SLD: super-luminescence diode array. L1-L6 – lenses. LP1,2- Linear polarizers. BS – beam splitter. G – transmission grating.

3. Results

A set of SEFC images at different depths close to the glass-blood interface shows (Fig. 2(a)) a strong reflection from the glass interface. At depths between 4μm and 8 μm images were still dominated by the reflection, but also included some featureless patterns due to the irregular flow at close proximity to the glass interface. Clear images of the blood cells were obtained only at depths larger than 10 μm. For many applications, using a pair of crossed polarizers could reduce surface reflections; however, crossed polarizers (see Fig. 1) were not used in our experiments because they have also removed the signal from the blood cells at all imaging depths (Fig. 2(b)) due to the preservation of light polarization in the blood. Typical SEFC

Biomedical Optics EXPRESS

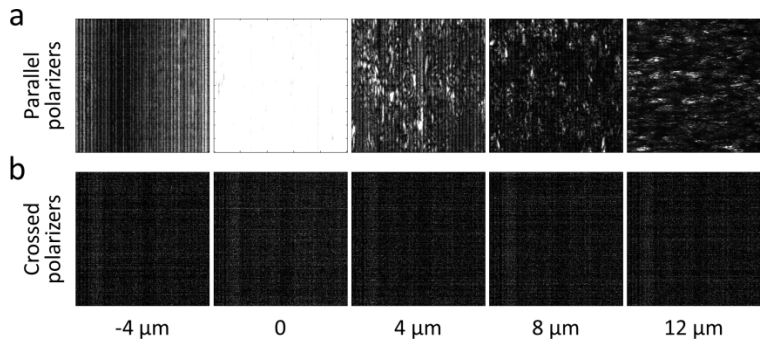

Fig. 2. SEFC images at different depths without (a) and with (b) crossed polarizers that remove the glass reflection completely but also eliminate the signals from the cells.

images of blood samples from our calibration set at 20%, 30%, 40%, 50% and 60% HCT are shown in Fig. 3 for different depths into the flow channel. The higher density of the RBCs at high HCT levels resulted in brighter SEFC images. Brightness was decreasing gradually with depth due to light scattering. Also note that the ratio between the wavelength encoded (horizontal) axis and the time (vertical) axis of individual cells was smaller at high imaging depths due to the higher flow velocity at regions that are distant from the glass wall. The

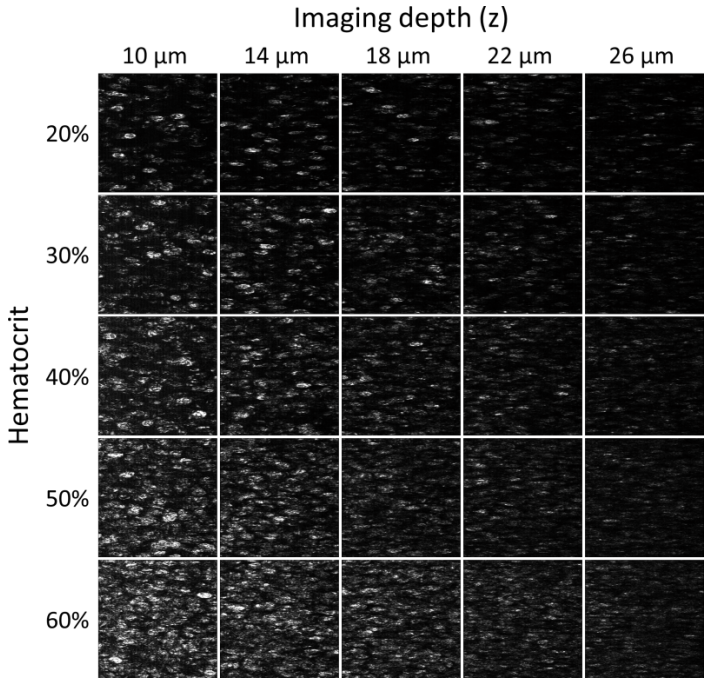

Fig. 3. SEFC images of blood at different depths for different hematocrit levels.

mean value of the pixel brightness (μ) of the SEFC images for different HCT levels and imaging depths is shown in Fig. 4(a). By plotting the HCT levels (Fig. 4(b)) as function of μ for a constant imaging depth of 14 µm, it was possible to fit the results with high accuracy (R^2 = 0.993) by a simple second-order polynomial. The fit was then used for estimating the HCT of the eight samples (Fig. 4(c)) with standard error of estimate of 1.7% simply by measuring the mean brightness of each sample at 14-µm depth and substituting the results in the

Biomedical Optics EXPRESS

polynomial equation. By plotting the averaged image brightness μ of each sample from our calibration set as a function of depth (Fig. 4(d)), good fits (R^2>0.98) to exponential decay rates were obtained for all HCT levels. Note however, that unlike in stationary measurements [20], the decay rates were decreasing for higher HCT levels (Fig. 4(e)), most likely due to the varying concentrations of the cells with depth due to the strong shear forces exerted by the glass interface at rapid flows. By excluding the lowest HCT levels (15% and 20%; hollow diamonds in Fig. 4(e)) the data was fitted by a linear curve (Fig. 4(e)), which was then used to estimate the HCT of the eight samples with standard error of estimate of 4.3% (Fig. 4(f)). Horizontal error bars in Figs. 4(c) and 4(f) represent the standard deviation of the centrifugation method [21]. Vertical error bars in 4c and 4f represent the error in the HCT measurement due to error in determining the exact imaging depth (1%) and in measuring the decay rates of the curves (2%).

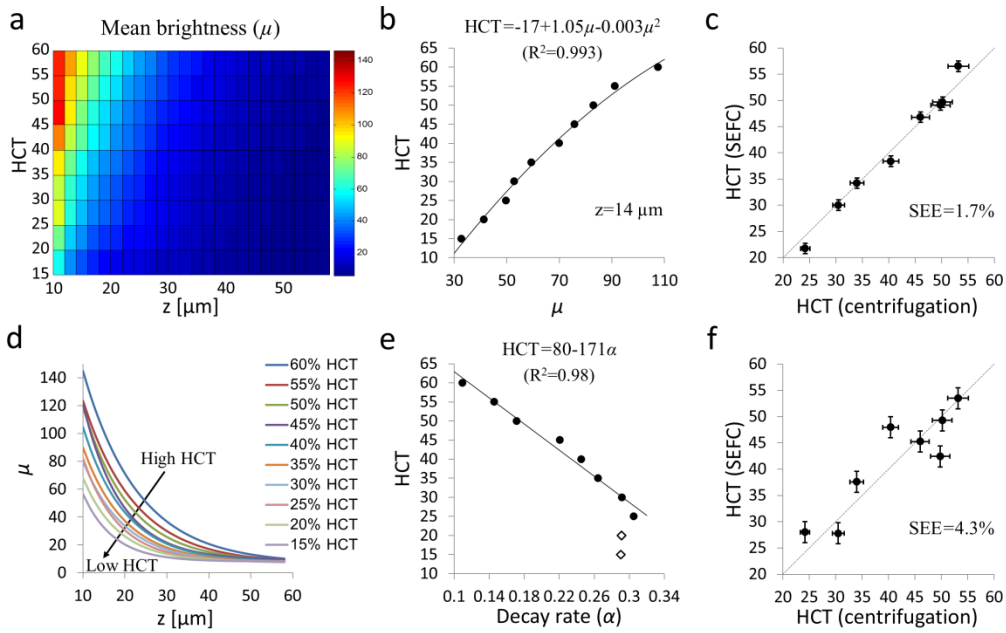

Fig. 4. (a) Mean images brightness (μ) for different HCT levels and imaging depths. (b) Mean brightness for different HCT levels at z = 14 µm. (c) Measured vs. control HCT of eight blood samples using the best fit equation in (b). (d) Mean image brightness as function of depth for different HCT levels. (e) HCT vs exponential decay rate. Hollow diamonds represent the lowest HCT levels that were excluded from the linear fit. (f) Measured vs. control HCT of eight samples using the decay rate equation in (e). SEE - Standard error of estimate.

Another parameter that correlates with the HCT is the coefficient of variation (c_v) of the SEFC images (i.e. the standard deviation of the pixel values (brightness) in each image (σ; Fig. 5(a)) divided by μ, Fig. 4(a)), which was calculated for each HCT of the calibration set (Fig. 5(b)) at different depths. The coefficient of variation correlates well with HCT because it reflects the sample inhomogeneity across the field of view; high HCT samples would exhibit uniform reflectance while low HCT samples would show high variance between the scattering cells and the dark plasma gaps between them. Using a similar procedure to that described in Fig. 4, an equation HCT(c_v) for a constant depth (14 µm), which best fitted the calibration data set in Fig. 5(b), was used to calculate HCT for the eight samples with standard error of estimate of 4.2% (Fig. 5(c)).

Biomedical Optics EXPRESS

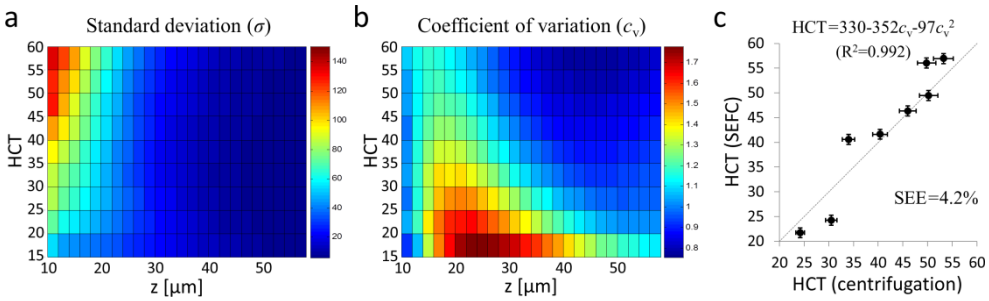

Fig. 5. Standard deviation (a) and coefficient of variation (b) of the SEFC image brightness for different HCT and imaging depths. (c) Measured vs. control HCT of eight samples using the coefficient of variation fit equation for 14 μm imaging depth. SEE- Standard error of estimate.

While the result analyses shown in Figs. 4-5 imply accuracy as high as 1.7% in the HCT measurement, the experimental procedure necessitated knowledge of the imaging depth with accuracy better than 1 μm; uncertainty of 1 μm in estimating the imaging depth corresponds to doubling the measurement error from 1.7% to 3.4%. In many applications, however, including point-of-care devices and *in vivo* measurements [17, 18], imaging depth is often unknown or cannot be accurately adjusted to sub-micron levels. In order to study a method for measuring HCT without prior knowledge of the exact imaging depth, we calculated both the mean image brightness and the coefficient of variation for every imaging depth with each HCT level (Fig. 6(a)). The shape of each curve in Fig. 6(a) is unique to a specific HCT level; as depth increases μ drops continuously, while c_v decreases with depth only for depths between 22 μm and 44 μm, where the curves are monotonic with unique slopes for each HCT levels. The data for the 22 μm - 44 μm depth range is plotted in Fig. 6(b), forming a three-dimensional surface that could be fitted by a fourth-degree polynomial that expresses the HCT as function of μ and c_v (Fig. 6(b)). By calculating μ and c_v from a single image acquired at an arbitrary, unknown depth (in the 22 μm - 44 μm range), we obtained HCT measurements (Fig. 6(c)) of the eight blood samples with a 4% standard error of estimate. Using multiple images acquired at different depths and averaging over the calculated μ and c_v parameters for all depth further improved the standard error of estimate to 3.5% (Fig. 6(d)). Vertical error bars in Fig. 6(c) and 6(d) represent the 2% standard deviation of the calibration curve. Horizontal error bars in 6c-d represent the standard deviation of the centrifugation method (0.5-2% [21]).

Biomedical Optics EXPRESS

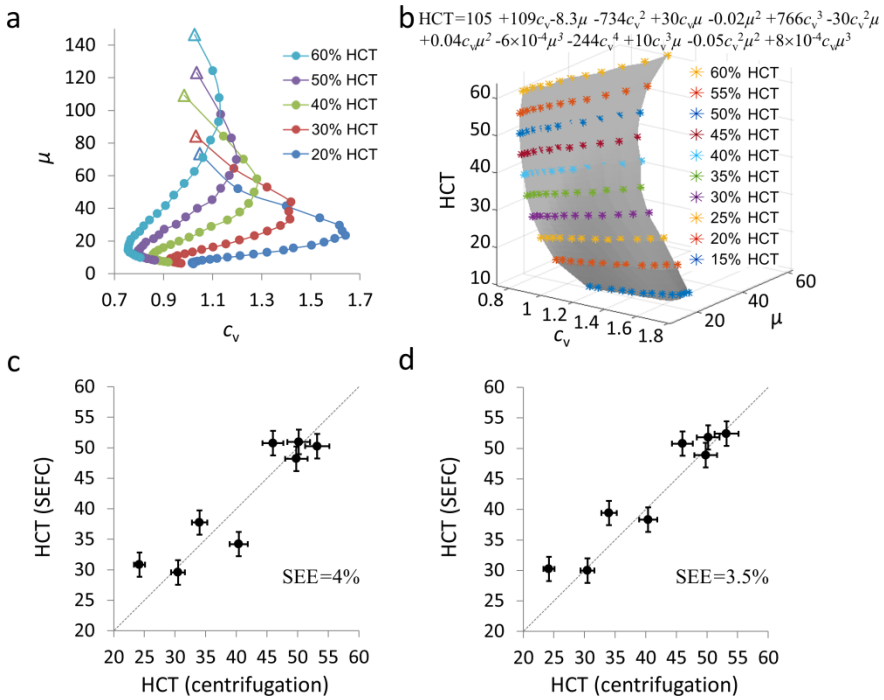

Fig. 6. (a) Mean image brightness vs. the coefficient of variation for different HCT levels. The data point corresponding to the shallowest depth (10 μm) is marked by hollow triangles. Depth intervals between neighboring points are 2 μm. (b) Three-dimensional surface representing HCT as function of μ and c_v for the 22 μm - 44 μm depth range. (c) Measured vs. control HCT of eight samples using the fit equation in (b) for a single image captured at an arbitrary depth. (d) Same as (c), with averaging over multiple images acquired at different depths with 2 μm intervals. SEE - Standard error of estimate.

4. Discussion

In reflectance confocal imaging of blood, the amount of light reflectance is strongly affected by the cell's density that is directly correlated with the blood HCT level. By calculating the average brightness and the coefficient of variation from the SEFC raw images of blood samples, we demonstrated HCT measurements with standard error of estimate between 1.7% and 4.3%, depending on the analysis approach. Generally, blood samples with higher HCT levels resulted in a higher total reflected signal (Fig. 4(a)-4(b)) and in a lower coefficient of variation (c_v, Fig. 5(b)). Both of these parameters exponentially decay as a function of the depth; however, perhaps counterintuitively (unlike in Ref [21].), the decay rate of the mean brightness value μ decreases with increasing HCT levels. This is most likely due to the effect of the flow – the density of cells increases gradually from zero at the glass interface to a maximum at the center of the flow channel. This density gradient implies that scattering is not uniform as function of depth, hence preventing the application of a simple Beer-Lambert law (that requires uniform scattering coefficient). Moreover, as HCT is not a monotonic function of the decay rates α, it was not possible to find a one-to-one correlation between them (α = 0.28 for both 15% and 30% HCT, for example).

While the imaging depth is a critical parameter for measuring HCT, it would often be difficult to measure or to maintain constant during measurement. In certain potential applications at the point of care, plastic disposable flow chambers or low-cost focusing controllers could result in inaccurate depth estimation of the order of several microns. By using both μ and c_v parameters we identified a unique parameter space in which each HCT level is different from other levels regardless of the measurement depth. This method allowed

Biomedical Optics EXPRESS

us to assign a specific HCT level to each (μ, c_v) pair calculated from a single SEFC image at unknown depth.

Perhaps the key for achieving high accuracy in the presented HCT measuring technique is the need for careful calibration measurements. In our experiment, calibration samples with different HCT levels were obtained by mixing the blood plasma with the RBC pellet that was assigned a 100% HCT value. Unfortunately, obtaining pellets of 100% HCT is not always practical due to the presence of residual trapped plasma within the RBC pellet [22], resulting in an unknown overestimation of the HCT of the calibration curves. Repeating calibration experiments would most likely be required in any future implementation of this method to account for the specific imaging (signal power, imaging depth) and flow (velocity, flow chamber geometry) conditions.

In summary, a method for *in vitro* HCT measurement with high accuracy was demonstrated using high-resolution reflectance confocal imaging of blood cells in flow. Measuring hematocrit with SEFC may not necessarily be more accurate or less costly compared to existing methods; its main strength would stem from its potential to measure, in addition to hematocrit, numerous other valuable blood parameters, including RBC, MCV, red blood cell distribution width (RDW) and differential white blood cell count. Such multi-parameter measurement would be useful for patient diagnosis at the point of care using a small blood sample.

Funding

The study was funded in part by the Israel Science Foundation grant (651/14). This work was also supported in part by the Lorry I. Lokey Interdisciplinary Center for Life Sciences and Engineering.